UNIVERSIDAD NACIONAL DE COLOMBIA

Extensión de la descomposición de energía para el análisis de mecanismos de reacción dentro de la teoría de fuerza y flujo electrónico de reacción

Matheus Rodríguez Álvarez

Universidad Nacional de Colombia
Departamento de Química
Bogotá, Colombia
2015

Extensión de la descomposición de energía para el análisis de mecanismos de reacción dentro de la teoría de fuerza y flujo electrónico de reacción

Matheus Rodríguez Álvarez

Tesis o trabajo de grado presentada(o) como requisito parcial para optar al título de:
Magister en Ciencias Química

Director(a):
Ph.D. Andrés Reyes Velasco

Línea de Investigación:
Química Cuántica
Grupo de Investigación:
Química Cuántica y Computational

Universidad Nacional de Colombia
Departamento de Química
Bogotá, Colombia
2015

Extension of the energy decomposition analysis for reaction mechanisms within force and electronic flux theories

Matheus Rodríguez Álvarez

Universidad Nacional de Colombia
Chemistry Department
Bogotá, Colombia
2015

Extension of the energy decomposition analysis for reaction mechanisms within force and electronic flux theories

Matheus Rodríguez Álvarez

Thesis presented in partial fulfillment of the requirements for the Degree of:
Master in Sciences - Chemistry

Advisor:
Ph.D. Andrés Reyes Velasco

Research Area:
Quantum Chemistry
Research Group:
Quantum and Computational Chemistry

Universidad Nacional de Colombia
Chemistry Department
Bogotá, Colombia
2015

Dedicated to my two moms, they are the girls behind the scene.

"There is no such thing as teaching without research and research without teaching"

["No hay enseñanza sin investigación ni investigación sin enseñanza."]

Paulo Freire

Acknowledgements

First of all, I would like to express my sincere gratitude to my advisor, Prof. Andres Reyes, for his support, immense patience and for allowing me to realize how vast the quantum chemistry world is.

I deeply acknowledge my labmates in Quantum and Computational Chemistry group at Universidad Nacional de Colombia, for the coffee, pizza, lunch, football, bike and stimulating discussion times. In particular, I am indebted to Jorge Charry, without his support and problem solving skills it would not be possible to conduct this research.

My sincere thanks to Jonathan Romero for sharing his experience and the encouraging discussions about science and music. I also thank to Johan Galindo for his advices in the writing process and friendship. I am grateful to Danilo, Ronald, Laura, Mauro, Alejo, Isma, Carlos and Nefta each one of them know the reasons.

Last but not the least, I would like to thank my family and Mónica. Without my mother Eugenia and my cousin Lilia the way to this moment would be impossible. I also thank to my grandparents Ana and Juan, unfortunately life comes and goes very fast. I thank to Mónica, it has been a short time but a strong support and company. Finally my thanks to Estrella that can only read these words with her heart.

Resumen

En éste trabajo se presenta la extensión teórica del método de descomposición de energía por densidades Grid-EDA. Esta extensión se realizó bajo la metodología del orbital molecular para cualquier partícula (APMO) a un nivel de teoría Hartree-Fock (HF). La implementación del método de descomposición de energía se realizó en el paquete computacional de química cuántica LOWDIN. Esta metodología fue aplicada para el estudio de una reacción de doble transferencia protónica en el dímero de ácido fórmico y seis sistemas positrónicos. Los resultados obtenidos demuestran que Grid-EDA y Grid-EDA-APMO ofrecen una explicación química cualitativa de los procesos de enlace químico a través de los cambios en las energías atómicas.

Palabras clave: LOWDIN, APMO, Método de descomposición de energía por densidades (EDA), Doble transferencia protónica, dímero de ácido fórmico, positrones.

Abstract

In this work we present the implementation, and theoretical extension of the energy density analysis method Grid-EDA within the any particle molecular orbital approach APMO, at Hartree-Fock (HF) level of theory. The implementation of the energy decomposition method for regular electronic structure systems, and molecular systems with different type of quantum species, was coded in the LOWDIN computational package. Our method was applied to study a double proton transfer reaction in formic acid dimer and six positronic systems. The results from Grid-EDA and Grid-EDA-APMO/HF show a qualitative explanation of chemical binding processes throughout atomic energy changes.

Keywords: LOWDIN, APMO, Energy Density Analysis (EDA), Double proton transfer, formic acid dimer, positrons.

Contents

Acknowledgements xi

Summary xiii

1 Introduction 2

2 Theoretical Background 4
- 2.1 Mulliken-type EDA . . . 4
  - 2.1.1 Atomic Mulliken-type EDA . . . 6
- 2.2 Grid-EDA . . . 7
  - 2.2.1 APMO . . . 10

3 Theoretical extension of Grid-EDA and computational implementaion in LOWDIN 12
- 3.1 Theoretical development . . . 12
- 3.2 Implementation in LOWDIN program . . . 13
- 3.3 Grid-EDA and Grid-EDA-APMO/HF implementation . . . 13
  - 3.3.1 Grid-EDA . . . 13
  - 3.3.2 Grid-EDA-APMO/HF . . . 14
  - 3.3.3 EDA Workflow in LOWDIN . . . 16
- 3.4 Validation . . . 18
  - 3.4.1 Grid points test . . . 21
  - 3.4.2 Atomic radii tests . . . 23
  - 3.4.3 Code optimization . . . 25

4 Applications 28
- 4.1 Grid-EDA application . . . 28
- 4.2 Grid-EDA-APMO/HF application . . . 36

5 Conclusions and perspectives 40

Bibliography 42

1 Introduction

Processes like bond breaking-formation, hydrogen bonds, isomerization, proton transfer, among others, have driven chemists over centuries to formulate series of concepts to explain what happens within a molecule when any of these phenomena occcur [1],[2]. Although concepts in chemistry are poweful tools for understanding these procesess, they lack of physical support for local effects like steric hindrance, atomic density delocalization, charge transfer between atoms etc. since these effects are not observables [3].

Those chemical unobservable interactions can be analyzed with quantum chemistry in several ways: using wave function, density matrices, or decomposing the total molecular energy into a sum of atomic or region contributions with schemes named Energy decomposition analysis methods (EDAM) [4, 5, 6, 7, 8, 9].

The EDAM are classified whether they use Hilbert space of atomic orbitals or 3D geometrical molecule partition to divide the ground state molecular energy [7]. Particular examples of those methods are the energy decomposition analysis proposed by Su et al. [4] and Kitaura-Morokuma [5], decomposition methods using Atoms in Molecules (AIM) [6], fuzzy atoms [7] and the Energy Density Analysis (EDA)[8, 9].

The total energy of a molecular system is a fundamental observable in quantum chemistry calculations and its decomposition varies with respect to the EDAM election. Even there is not a unique EDAM that explains all chemistry phenomena, it is desirable to select a decomposition scheme less dependent on subjective criteria and deep theoretical background of the method, additionally it is important that numerical results can be associated with chemical descriptive picture.

From EDAM, two promising decomposition schemes have been proposed; the Mulliken-type EDA [8], which is analogous to Mulliken Population analysis, and the numerical based approach Grid-EDA that divides the total energy of the system into atomic energy density contributions[9]. These two methods have a direct way to connect the results to chemical phenomena and combine them with other theories to enhance their analysis features [10, 11, 12, 13, 14, 15]. These EDA methods have been useful to study Diels-Alder reactions [16], metal clusters [17] [18], charge transfer in lithium batteries [19], proton transfer [20] and they were considered as a variable of principal component analysis to evaluate anti HIV activity in a set of coumarines[21], besides other appplications.

Notwithstanding the large variety of EDAM for regular electronic structure calculations, non-conventional molecular systems lack of this type of methods to explain interactions like nuclear quantum effects (NQE) or positrons with molecules. In this regard, some energy

decomposition analysis are presented to particular (non-conventional) systems [22] but there is not a generalized method to treat these phenomena.
Series of methodologies called Multi-Component Molecular Orbital method (MCMO)[23], Nuclear Orbital plus Molecular Orbital method (NOMO)[24] and Nuclear-Electronic Orbital (NEO)[25] were initially proposed to study NQE; nonetheless the study of other quantum particles within molecular systems like positrons or muons have gained an increasing research interest [26, 27]. The Any Particle Molecular Orbital Approach (APMO)[28] was developed to treat multiple types of quantum species, when APMO is used at Hartree-Fock level of theory it is called APMO/HF. APMO has been used succesfully to study NQE [29, 30], muons [31, 32] and positrons [33], [34] in molecular systems. This approach is implemented in LOWDIN software package[35].
In this work, we present the theoretical extension of Grid-EDA method to any particle under APMO approach (Grid-EDA-APMO/HF), this theoretical extension is (to the best of our knowledge) the first energy decomposition analysis method extended to treat any type of quantum species. We implement Grid-EDA and Grid-EDA-APMO/HF methodologies in LOWDIN package, after the implementation, we present applications of double proton transfer process in formic acid dimer, and positronic diatomic molecules. For both applications, these decomposition methodologies are promising tools to analise chemical binding procesess.

2 Theoretical Background

The energy density analysis methods can be classified in two goups, Mulliken-type EDA and Grid-EDA, both schemes decompose the total molecular energy into atomic energy density contributions. In this chapter we present the equations for EDA-type Mulliken [8] and Grid-EDA [9] methods, we also include the APMO equations which are the basis to treat multiple quantum species.

2.1 Mulliken-type EDA

For the total energy under HF approach we have :

$$^{Tot}E = E_{NN} + E_T + E_{NE} + E_{CLB} + E_{HFx}, \tag{2-1}$$

where E_{NN} is the nuclear repulsion energy and is defined as

$$E_{NN} = \frac{1}{2}\sum_{AB}\frac{Z_A Z_B}{\mid R_A - R_B \mid}, \tag{2-2}$$

where Z_A, Z_B and R_A, R_B are nuclear charges and coordinates for A^{th} and B nuclei.
E_T is the kinetic energy which is represented by:

$$E_T = \sum_{\mu\nu} P_{\mu\nu} T_{\nu\mu}, \tag{2-3}$$

where $P_{\mu\nu}$ is an element of electronic density matrix, $T_{\nu\mu}$ is an element of kinetic matricial operator and μ, ν indices run over atomic orbitals.
The nuclear-electron attraction E_{NE} is

$$E_{NE} = \sum_{\mu\nu}\sum_{A} P_{\mu\nu} V_{\nu\mu,A}, \tag{2-4}$$

where $V_{\nu\mu,A}$ is an element of potential energy matrix and μ, ν indices run over atomic orbitals. The sum over A represents the sum for all A atoms in the system.

The Coulombic term E_{CLB} is a product between the density matrix P and the Coulomb operator $\hat{J}$:

$$E_{CLB} = \sum_{\mu\nu} P_{\mu\nu} J_{\nu\mu}, \tag{2-5}$$

the indices μ and ν run over atomic orbitals.
The exchange energy is defined as:

$$E_{HFx} = \sum_{\mu\nu} P_{\mu\nu} K_{\nu\mu} \tag{2-6}$$

where $K_{\nu\mu}$ is a matricial element of the exchange operator $\hat{K}$.
For Density Functional Theory (DFT) the total energy is

$$E^{Tot} = E_{NN} + E_T[\rho] + E_{NE}[\rho] + E_{CLB}[\rho] + {}^{grid}E_{DFTxc}[\rho], \tag{2-7}$$

the only difference with HF corresponds to the term ${}^{grid}E_{DFTxc}[\rho]$, which is the exchange-correlation functional energy. This functional energy is calculated using numerical quadratures with Becke's space-partitioning function [36],

$${}^{grid}E_{DFTxc}[\rho] = \sum_A \sum_g \omega_g p_A(r_g) F_{xc}(rg), \tag{2-8}$$

where $F_{xc}(rg)$ is the exchange-correlation functional, ω_g and p_A are the weight Becke's space-partitioning function and g runs over grid points. The integration is determined by a Lebedev grid that uses Euler-Maclaurin scheme for the radial part and Gauss-Legendre scheme for the angular part [37].
Becke's space-partitioning function p_A aims to reduce the problem of three dimensional molecular integration to atomic weighted contributions that must satisfy the following fundamental conditions:

$$p_A(r) \geq 0 \tag{2-9}$$

and

$$\sum_A p_A(r) = 1. \tag{2-10}$$

This partitioning scheme has a value of one in the vicinity of the A^{th} nucleus but vanishes smoothly near any other nuclei [36].

2.1.1 Atomic Mulliken-type EDA

Analogous to Mulliken population Analysis (MPA) -that calculates the atomic population as product between density and overlap matrices- [38], Nakai [8] proposes the decomposition of the total atomic energy as follows:

$$E_{tot}^{A} = E_{NN}^{A} + E_{T}^{A} + E_{Ne}^{A} + E_{clb}^{A}, \tag{2-11}$$

where E_{NN}^{A} is the nuclear repulsion for the A^{th} nucleus and its expresion is

$$E_{NN}^{A} = \frac{1}{2} \sum_{B \neq A} \frac{Z_A Z_B}{\mid R_A - R_B \mid}. \tag{2-12}$$

The atomic kinetic energy density for the A^{th} atom is:

$$E_{T}^{A} = \sum_{\mu \in A, \nu} P_{\mu\nu} T_{\nu\mu}. \tag{2-13}$$

where the variables are the same for molecular system and the atomic orbitals are restricted to the A^{th} atom.
In the atomic nuclear-electron attraction,

$$^{Mull}E_{NE}^{A} = \underbrace{\frac{1}{2} \sum_{\mu \in A, \nu} \sum_{B} P_{\mu\nu} V_{\nu\mu,B}}_{\text{V1}} + \underbrace{\frac{1}{2} \sum_{\mu\nu} P_{\mu\nu} V_{\nu\mu,A}}_{\text{V2}}, \tag{2-14}$$

the equation is grouped into V1 and V2 terms where V1 represents the attraction potential between the A^{th} atomic electrons and B nuclear potentials and V2 is the potential between the electrons of B nuclei and A^{th} nucleus.
The Coulomb and exchange atomic energy densities are

$$^{Mull}E_{CLB}^{A} = \sum_{\mu \in A, \nu} P_{\mu\nu} J_{\nu\mu}, \tag{2-15}$$

and

$$^{Mull}E_{HFx}^{A} = \sum_{\mu \in A, \nu} P_{\mu\nu} K_{\nu\mu}, \tag{2-16}$$

where atomic orbitals belong to atom A^{th}, $P_{\mu\nu}$ is an element of density matrix, $\hat{J}$ and $\hat{K}$ are Coulomb and exchange matricial operators.

For density functional theory the atomic total energy density is decomposed as

$$^{Mull}E^{A}_{tot} = ^{Mull}E^{A}_{NN} + ^{Mull}E^{A}_{T} + ^{Mull}E^{A}_{Ne} + ^{Mull}E^{A}_{clb} + ^{Grid}E^{A}_{DFTxc}[\rho], \tag{2-17}$$

where $^{Grid}E^{A}_{DFTxc}[\rho]$ corresponds to the exchange-correlation functional atomic energy and is defined by

$$^{grid}E^{A}_{DFTxc}[\rho] = \sum_{g} \omega_g p_A(r_g) F_{xc}(rg), \tag{2-18}$$

where ω_g and $p_A(r_g)$ are the weight and Becke's space-partitioning function and the sum runs over grid points g. For a proper molecular space division in heteronuclear systems the atomic size adjustment was computed with the Bragg-Slater radii [39].

2.2 Grid-EDA

Grid-EDA is an energy decomposition method based on molecular spatial division, following Becke's space partitioning function used to calculate the exchange-correlation functional in DFT. The use of numerical quadratures is extended to HF kinetic, Coulomb and exchange energy densities.
This method decreases the strong basis set dependence of Mulliken-type EDA, furthermore this numerical approach (Grid-EDA) overcomes the limitations of Mulliken-type EDA where this scheme fails to yield reasonable physical results e.g. metalic clusters [9].
The energy components of Grid-EDA for the total molecular energy and the total atomic energy are shown in the following mathematical description. For molecular and atomic nuclear-nuclear repulsion we have the equations 2-2 and 2-12. The kinetic molecular energy is represented by

$$^{grid}E_{T} = \sum_{A}\sum_{g} \omega_g p_A(rg) \sum_{\mu\nu} P_{\mu\nu}\chi^{*}_{\nu}(rg)\left(-\frac{1}{2}\nabla^2\right)\chi_{\mu}(rg), \tag{2-19}$$

where ω_g and $p_A(rg)$ are the weight and Becke's space-partitioning function, the first sum runs over atoms A of the molecular system and the second sum runs over the number of grid points g, rg corresponds to the spatial grid coordinates, P is the density matrix, χ are the atomic orbitals and the indices μ, ν run over all atomic orbitals.
The kinetic energy density for an A atom is

$$^{grid}E^{A}_{T} = \sum_{g} \omega_g p_A(rg) \sum_{\mu\nu} P_{\mu\nu}\chi^{*}_{\nu}(rg)\left(-\frac{1}{2}\nabla^2\right)\chi_{\mu}(rg). \tag{2-20}$$

The nuclear-electron molecular attraction corresponds to

$$^{grid}E_{NE} = \sum_{A}\sum_{B}\sum_{g}\omega_g p_B(r_g)\frac{-Z_A}{\mid r_g - R_A \mid}\rho(r_g), \tag{2-21}$$

in this expression $\rho_B(r_g)$ is the grid density for B atoms in the molecule and $\rho(r_g)$ corresponds to the total grid density.
For a given atom A, the nuclear-electron attraction is

$$^{grid}E^{A}_{NE} = \underbrace{\frac{1}{2}\sum_{B}\sum_{g}\omega_g\rho_B(r_g)\frac{-Z_A}{\mid r_g - R_A \mid}\rho(r_g)}_{\text{Vg1}} + \underbrace{\frac{1}{2}\sum_{B}\sum_{g}\omega_g\rho_A(r_g)\frac{-Z_B}{\mid r_g - R_B \mid}\rho(r_g)}_{\text{Vg2}}, \tag{2-22}$$

where Vg1 is the attraction of the A nucleus with the electrons of B atoms and Vg2 is the attraction between the electrons of the A nucleus and B nuclei.
Finally we have the two-body interactions i.e. Coulomb and exchange energy density terms. To evaluate these terms it is necessary to calculate six-dimensional (6D) integrals as follows:

$$^{6D}E_{CLB} = \frac{1}{2}\sum_{A}\sum_{B}\sum_{g1}\sum_{g2}p_A(r_{g1})p_B(r_{g2})\omega_{g1}\omega_{g2} \times \sum_{\mu\nu\lambda\sigma}P_{\mu\nu}P_{\lambda\sigma}\frac{\chi_\nu(rg1)^*\chi_\mu(rg2)\chi^*_\sigma(rg2)\chi_\lambda(rg1)}{\mid r_{g1} - r_{g2} \mid}\rho(r_g), \tag{2-23}$$

and

$$^{6D}E_{HFx} = \frac{1}{4}\sum_{A}\sum_{B}\sum_{g1}\sum_{g2}p_A(r_{g1})p_B(r_{g2})\omega_{g1}\omega_{g2} \times \sum_{\mu\nu\lambda\sigma}P_{\mu\nu}P_{\lambda\sigma}\frac{\chi_\nu(rg1)^*\chi_\lambda(rg1)\chi^*_\sigma(rg2)\chi_\mu(rg2)}{\mid r_{g1} - r_{g2} \mid}\rho(r_g), \tag{2-24}$$

where $g1$ and $g2$ are the grid points for two different electrons. Equations 2-23 and 2-24 present singularities since $g1$ can be equal to $g2$; therefore, the numerical integration errors increase. To overcome this problem Nakai has used the pseudospectral (PS) method[40].
In PS method the Coulomb and exchange terms are evaluated numerically with respect to one coordinate and analytically with respect to the other. The elimination of singularities is supposed to have higher accuracy than the results of full numerical integration.

The equations for the total molecular energy applying PS to Coulomb and exchange interactios are:

$$^{PS}E_{CLB} = \frac{1}{2}\sum_{A}\sum_{g}\omega_g p_A(r_g)\sum_{\mu\nu}P_{\mu\nu}\chi^*_\nu(r_g)\chi_\mu(r_g)\sum_{\lambda\sigma}P_{\lambda\sigma}A_{\sigma\lambda}(r_g) \tag{2-25}$$

$$^{PS}E_{HFx} = \frac{1}{4}\sum_{A}\sum_{g}\omega_g p_A(r_g)\sum_{\mu\nu\lambda\sigma}P_{\mu\nu}P_{\lambda\sigma}\chi^*_\nu(r_g)\chi_\lambda(r_g)A_{\sigma\nu}(r_g) \tag{2-26}$$

$$A_{\mu\nu}(r_g) = \int \frac{\chi^*_\mu(r_2)\chi_\nu(r_2)}{\mid r_2 - r_g \mid}dr_2, \tag{2-27}$$

where A is an overlap integral with special points, this integral evaluates $r2$ analitically and $r1$ numerically,in the next equation $r1$ corresponds to rg.
The partition per atoms for Coulomb and exchange terms are:

$$^{PS}E^A_{CLB} = \frac{1}{2}\sum_{g}\omega_g p_A(r_g)\sum_{\mu\nu}P_{\mu\nu}\chi^*_\nu(r_g)\chi_\mu(r_g)\sum_{\lambda\sigma}P_{\lambda\sigma}A_{\sigma\lambda}(r_g) \tag{2-28}$$

$$^{PS}E_{HFx} = \frac{1}{4}\sum_{g}\omega_g p_A(r_g)\sum_{\mu\nu\lambda\sigma}P_{\mu\nu}P_{\lambda\sigma}\chi^*_\nu(r_g)\chi_\lambda(r_g)A_{\sigma\nu}(r_g). \tag{2-29}$$

The total molecular energy in HF with Grid-EDA is:

$$^{Grid-EDA}E^{Tot} = E_{NN} +^{grid} E_T +^{grid} E_{NE} +^{PS} E_{CLB} +^{PS} E_{HFx} \tag{2-30}$$

and the total atomic energy for an A^{th} atom is

$$^{Grid-EDA}E^{A} = E^A_{NN} +^{grid} E^A_T +^{grid} E^A_{NE} +^{PS} E^A_{CLB} +^{PS} E^A_{HFx}. \tag{2-31}$$

For DFT the total molecular

$$^{Grid-EDA}E^{Tot} = E_{NN} +^{grid} E_T[\rho] +^{grid} E_{NE}[\rho] +^{PS} E_{CLB}[\rho] +^{grid} E_{DFTxc} \tag{2-32}$$

and atomic energies are given by

$$^{Grid-EDA}E^{A} = E^A_{NN} +^{grid} E^A_T[\rho] +^{grid} E^A_{NE}[\rho] +^{PS} E^A_{CLB}[\rho] +^{grid} E^A_{DFTxc}. \tag{2-33}$$

The sum of the atomic energy densities yields the total energy

$$^{grid}E^{Tot} = \sum_{A}^{grid} E^{A}. \tag{2-34}$$

Finally the population obtained by Becke's partitioning function is:

$$^{grid}N^{A} = \sum_{g} \omega_g p_A(r_g)\rho(r_g), \tag{2-35}$$

these populations do not present the strong basis set dependece of Mulliken populations.

2.2.1 APMO

APMO allows the study of molecular systems including two or more types of quantum species [28]. The hamiltonian for a system with multiple types of quantum species and classical nuclei is

$$H = -\sum_{i=1}^{N^q} \frac{1}{2M_i}\nabla_i^2 + \sum_{i=1}^{N^q}\sum_{i>j}^{N^q} \frac{Z_i^q Z_j^q}{r_{ij}} + \sum_{i=1}^{N^q}\sum_{i=1}^{N^c} \frac{Z_i^q Z_j^c}{r_{ij}} + \sum_{i=1}^{N^c}\sum_{i>j}^{N^c} \frac{Z_i^c Z_j^c}{r_{ij}}, \tag{2-36}$$

where the first term is the kinetic energy of quantum particles, the second term refers to interactions within quantum particles pairs with Z_i^q and Z_j^q charges, the third term is the interaction between one classical and one quantum particles with Z_i^q and Z_j^c charges, and the last term is the interaction potential between classical particles with Z_i^c and Z_j^c charges. At APMO/HF level of theory the ground state wave function Ψ_0, is built as a Hartree product of wave functions ϕ^α of $N^{species}$ quantum species

$$\Psi_0 = \prod_{\alpha}^{N^{species}} \phi^\alpha. \tag{2-37}$$

For fermionic particles each ϕ^α is represented with an Slater determinant built with molecular spin-orbitals (MO) ψ_a^α.
Each orbital ψ_i^α is obtained solving Fock equations:

$$f^\alpha(i)\psi_i^\alpha = \varepsilon_i^\alpha \psi_i^\alpha, \qquad i = 1, \ldots, N^\alpha \qquad \alpha = 1, \ldots, N^{species}. \tag{2-38}$$

the effective Fock operator for one particle is

$$f^\alpha(i) = h^\alpha(i) + \sum_{j}^{N^\alpha} Z_\alpha^2 \left[J_j^\alpha - k_j^\alpha\right] + \sum_{\beta>\alpha}^{N^{species}} \sum_{j}^{N^\alpha} Z^\alpha Z^\beta J_j^\beta, \tag{2-39}$$

where $h(i)$ is the one-particle operator, Z^{α} and Z^{β} are the charges for α and β species, J_j^{α} and K_j^{α} are the Coulomb and exchange operators for electrons and J_j^{β} is the Coulombic interaction between different quantum species. This theory is implemented in LOWDIN computational package [35].

3 Theoretical extension of Grid-EDA and computational implementaion in LOWDIN

In this chapter we present the theoretical extension of Grid-EDA and its implementation in LOWDIN. For the implementation of Grid-EDA in regular electronic structure systems we followed an analogous validation scheme proposed in Nakai's work[9]. Finally we show a reduction in computing time for the code using an screening technique.

3.1 Theoretical development

The theoretical extension of Grid-EDA under APMO approach at HF level of theory is (to the best of our knowledge) the first energy decomposition analysis method extended to treat any type of quantum species. In this section we show the equations for the coupling energy term in the Grid-EDA-APMO/HF method, since this term involves the different kind of particles.

Grid-EDA-APMO/HF:

In the APMO approach the coupling term calculates the interaction between different quantum species. We added this term to the general expression for the total atomic energy in Grid-EDA (equation 2-31) once we added this term the general expression for the atomic energy in GRID-EDA-APMO/HF is:

$$^{APMO-Grid}E^A_{tot} = E^A_{NN} +^{grid} E^A_T +^{grid} E^A_{Ne} +^{PS} E^A_{clb} +^{PS} E^A_{HFx} +^{PS} E^A_{coup}, \tag{3-1}$$

where the first term is the A^{th} center repulsion energy, the second term refers to kinetic energy, the third term is A^{th} center-electron attraction, fourth and fifth terms are Coulomb and exchange energies respectively and the last term is the interaction energy between different quantum species or coupling term.

The Coupling Grid-EDA-APMO/HF term:

We define the coupling analytical expression for two types of quantum species α and β per atom as follows,

$$E^{A}_{\text{coupling}} = \sum_{\mu\nu}\sum_{\lambda\sigma} P_{\mu\nu}P_{\sigma\lambda}\int\int \frac{\chi^{*}_{\mu}(r_\alpha)\chi_{\nu}(r_\alpha)\chi^{*}_{\sigma}(r_\beta)\chi_{\lambda}(r_\beta)}{r_{\alpha\beta}} dr_\alpha dr_\beta \tag{3-2}$$

where the subscripts μ, ν are orbital indices for α species, λ, σ are orbital indices for β species, χ are orbitals and P is the density matrix.
This analytical expression would lead to a six-dimensional integral that present singularities in its solution, causing an increase in the integration errors. To overcome this problem, and based on Nakai's work [9], we propose to use a hybrid analytical-numerical solution using the pseudo-spectral method (Equations 2-25 and 2-26).
For A^{th} atom, the analytical-numerical expression of coupling term is:

$${}^{PS}E^{A}_{\text{coupling}} = \underbrace{\sum_{g^\alpha}\sum_{\mu\nu} \omega_{g^\alpha}\rho_A(r_{g^\alpha})P_{\mu\nu}}_{\alpha \quad species} \times \underbrace{\sum_{\lambda\sigma} P_{\sigma\lambda}\int \frac{\chi^{*}_{\sigma}(r_\beta)\chi_{\lambda}(r_\beta)}{r_\beta - r_{g^\alpha}} dr_\beta,}_{\beta \quad species} \tag{3-3}$$

this equation can be grouped in two parts, the first part depends on α quantum species and the second part depends on β quantum species. For α species we have the numerical solution with Becke's partitioning function, and for β species we have the analytical solution.

3.2 Implementation in LOWDIN program

LOWDIN is a software package that has several electronic structure methods such as Hartree-Fock, Møller-Plesset, configuration interactions, propagator theory, and the essentials of DFT with extensions to auxiliary DFT[35]. Besides these methods LOWDIN is extended to treat multiple quantum species using the APMO approach [28]. The schematic representation of LOWDIN structure is in figure **3-1**

3.3 Grid-EDA and Grid-EDA-APMO/HF implementation

3.3.1 Grid-EDA

The implementation of Grid-EDA, is coded in the equations of section 2.2. For the numerical part, we used the Becke's partitioning function and Lebedev grids available in LOWDIN-PARAKATA interface [41]. Besides the equations implemented in LOWDIN, we added

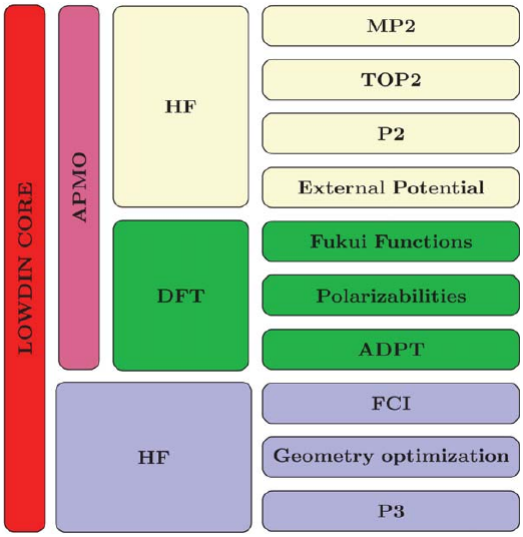

Figure **3-1**: LOWDIN global structure [35].

the Bragg-Slater radii [39] to adjust the energy partition in heteronuclear systems and we used the PS method to calculate the Coulomb and exchange atomic energy densities. All Grid-EDA equations were coded in the PDFt.f90 module of LOWDIN.

In LOWDIN, the input file is divided in the geometry, tasks and control sections. To use Grid-EDA method, we added the keyword *edaGrid* in control section. In figure **3-2** we present an example of the input file to run Grid-EDA calculations.

The summary of results in the output file is shown in figure **3-3**. The symbols in the figure from left to right are: the atoms, the populations obtained with Becke's partitioning function (Grid pop), the kinetic energy (Kinetic En.), the nuclear-electron attraction NE(nuc) and NE(elec) that corresponds to $Vg1$ and $Vg2$ in equation 2-22, the Coulomb and exchange interactions (JK), the total atomic energy and the atomic virial in the last column.

In the last part of this output we sum the energy terms. This sum facilitates the use of the program if the user wants to compare these numbers with the energy components of a HF calculation.

3.3.2 Grid-EDA-APMO/HF

For the extension of Grid-EDA to treat multiple quantum species, we implemented the coupling term (Equation 3-3) based on APMO approach, this term is added to Grid-EDA equations.

Examples of input and output files for Grid-EDA-APMO/HF calculations are shown in figures **3-4** and **3-5**

In this input file, we show a Grid-EDA-APMO/HF calculation of lithium hydride including one positron. The positron, e^+, for this example, is centered in the hydrogen nucleus with

```
 SYSTEM_DESCRIPTION='Water'

GEOMETRY
e-(O)       aug-cc-pVTZ          0.0000000    0.0000      0.1173
e-(H)       aug-cc-pVTZ         -0.0000000    0.7572     -0.4692
e-(H)       aug-cc-pVTZ          0.0000000   -0.7572     -0.4692
O           dirac                0.0000000    0.0000      0.1173
H           dirac               -0.0000000    0.7572     -0.4692
H           dirac                0.0000000   -0.7572     -0.4692
END GEOMETRY

TASKS
method = "RHF"
END TASKS

CONTROL
readCoefficients=F
        edaGrid = T
END CONTROL
```

Figure **3-2**: Input file for Grid-EDA calculation of water molecule.

```
================================================================================================================
                              Grid-EDA Atomic Energy Density Analysis
================================================================================================================
   Atom  Grid Pop.    NN rep      Kinetic En.   NE(nuc)      NE(elec)       JK          Total      Virial
   1O    8.171138     4.420052    74.836370   -93.737594   -94.125728    33.726079   -74.880820    2.000594
   2H    0.914431     2.384741     0.570824    -2.885789    -2.691722     2.031766    -0.590179    2.033906
   3H    0.914431     2.384741     0.570824    -2.885789    -2.691722     2.031766    -0.590179    2.033906

   ------------------------------------------------
    Grid-EDA Energy Components and Nuclear Repulsion:
   ------------------------------------------------

   TOTAL KINETIC ENERGY DENSITY =            75.978019
   TOTAL NE [NE(nuc)+NE(elec)]  =          -199.018342
   TOTAL COULOMB AND EXCHANGE   =            37.789610
   TOTAL NUCLEAR REPULSION      =             9.189534

================================================================================================================
                            END Grid-EDA Atomic Energy Density Analysis
================================================================================================================
```

Figure **3-3**: Results summary of Grid-EDA calculation in output file for water molecule

its positronic basis set [34].
In the output file we have the coupling energy decomposition for the positron with lithium

```
SYSTEM_DESCRIPTION='LiH with positron'

GEOMETRY
        e-(H)    aug-cc-pVTZ              0.000000    0.00000  0.000
        e-(Li)   aug-cc-pVTZ              0.000000    0.00000  1.669
        H        dirac                    0.000000    0.00000  0.000
        Li       dirac                    0.000000    0.00000  1.669
        e+       e+-H-7SPD-aug-cc-pVTZ    0.000000    0.00000  0.000
END GEOMETRY

TASKS
        method = "RHF"
END TASKS

CONTROL
        readCoefficients = F
        edaGrid=T
END CONTROL
```

Figure **3-4**: Input for Grid-EDA-APMO/HF calculation of LiH with one positron

and hydrogen atoms repectively (numbers 1 and 2 after GRID-EDA COUPLING label). The differences in coupling energies obtained with EDA-Grid-APMO/HF and a APMO/HF calculation are less than 1 kcal/mol in all tested systems **3-5**.

3.3.3 EDA Workflow in LOWDIN

In brief, the workflow of Grid-EDA and Grid-EDA-APMO/HF is shown in figure **3-6**. Our implementation receives the density matrix from HF or DFT, in the PDFt.f90 module. Within this module we have predetermined the grid parameters and the energy decomposition starts with our implementation which is in purple. Every atomic term does the atomic size adjustment that also was coded in PDFt.f90, finally we have the tables in the output file. The green block corresponds to possible new extensions of Grid-EDA with other methodologies.

```
================================================================================================
                              Grid-EDA Atomic Energy Density Analysis
================================================================================================
Atom  Grid Pop.    NN rep     Kinetic En.  NE(nuc)     NE(elec)    JK          Total     Virial
 1H   0.940814    0.475594    0.487114   -1.102466   -0.873267   0.498525  -0.514500    2.056221
 2Li  3.059058    0.475594    7.475837   -9.060590   -9.289789   2.928946  -7.470002    1.999220

   ---------------------------------------------------
    Grid-EDA Energy Components and Nuclear Repulsion:
   ---------------------------------------------------

   TOTAL KINETIC ENERGY DENSITY  =             7.962951
   TOTAL NE [NE(nuc)+NE(elec)]   =           -20.326112
   TOTAL COULOMB AND EXCHANGE    =             3.427471
   TOTAL NUCLEAR REPULSION       =             0.951187

************************************************
GRID-EDA COUPLING                1 -0.1465067246
************************
GRID-EDA COUPLING                2 -0.354162118

Coupling energy:
---------------
   e- Coupling energy  =        -0.5006565822
   e+ Coupling energy  =        -0.5006852551
************************************************
================================================================================================
                             END Grid-EDA Atomic Energy Density Analysis
================================================================================================
```

Figure **3-5**: Output for Grid-EDA-APMO/HF calculation of LiH with one positron

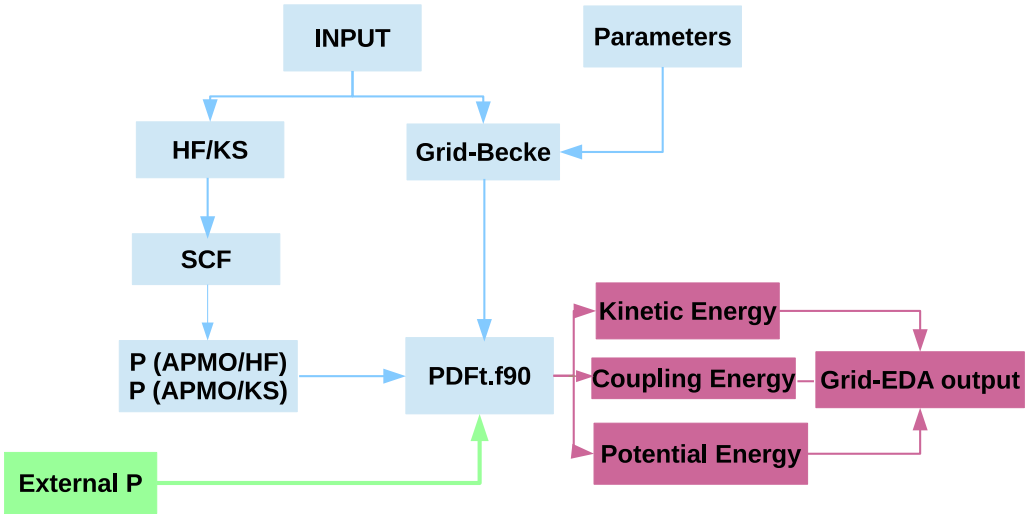

Figure **3-6**: Program workflow. Capital P corresponds to density matrix. Light color corresponds to determination of density matrix and grid parameters, the green part is a connection with other methodologies and the purple color corresponds to our implementation

We can describe the general algorithm as:

1. **LOWDIN HF or APMO/HF calculation:** From this calculation we obtain the density, kinetic, Coulomb and exchange matrices from Wavefunction_HF.f90 module, the nuclear-nuclear repulsion is calculated first with HF.

2. **Load information fom input file:** With the key word *edaGrid*, the program loads the particle charges and masses parameters. This information is loaded in the PDFt.f90 module that contains the subroutines for EDA-Grid and EDA-Grid-APMO/HF methods.

3. **Energy terms calculation:** PDFt.f90 module stablishes the number of grid points to use (22650 by default), based on this information, the operations between matrices for Grid-EDA and its extension under APMO approach begins in this order: Grid populations, atomic kinetic energy, two body interactions (JK), nuclear electron energy and coupling energy.

4. **Atomic size adjustment**: With Bragg-Slater atomic radii parameters, the program makes the atomic size adjustment for atomic energy partitions before the end of each subroutine.

5. **Print results** in Grid-EDA and Grid-EDA-APMO/HF table.

Finally it is important to notice that the bottleneck of the calculation in time computing relies on JK energy term.

3.4 Validation

Grid-EDA is only available in a personal version of GAMESS[42] that belongs to Nakai research group, for this reason a direct comparison of results between our implementation and an standard program can not be done. However, our validation in LOWDIN is possible since we follow an analogous analysis described in Grid-EDA paper [9]. Since LOWDIN lacks of density funcionals for regular electronic structure we did the analysis at HF level of theory.
This analysis considers the total energy obtained in a single point HF calculation as a reference value. The sum of the total atomic energy densities of Grid-EDA must recover the total energy reported by the HF calculation; if the difference between HF and Grid-EDA results is less than 1 kcal/mol the numerical assessment is suitable to describe chemical phenomena [9].
To validate the total energy partition obtained with Grid-EDA, Nakai et. al. compute the atomic energy percentages of the total energy and compare those results with Mulliken-type

EDA calculations. The purpose of this comparison is not to obtain the same numbers - as both schemes have significant differences- but to obtain similar percentages of atomic energies versus a standard method as Mulliken-type EDA. It is worth to mention that those comparisons must be done with no challenging systems since the former method has some limitations due to its strong basis set dependence.

We selected the G2/97 set of neutral molecules [43] to test our Grid-EDA implementation, this set of molecules were selected because it was the base to validate the EDA methods [8], [9]. Therefore, we computed the Grid-EDA method for water molecule with different basis sets, using the experimental geometry of water [44], after it, we performed the Mulliken-type EDA calculation in GAMESS with the same geometry, Table **3-1** shows the results of these calculations.

From these results, we have the total HF energy as the reference point to compare the energy partitions between Mulliken-type EDA and Grid-EDA, this computation shows for both EDA methods that we have approximately a 98% of the total energy for oxygen and more than 1% for hydrogen. Once we guarantee for this model system that the partition of energies is reasonable (based on total energies percentages), we calculate the energy differencies between Grid-EDA and HF calculations. The results in Table **3-2** shows that the differencies are within chemical accuracy independent of the basis set used. These results are similar for the subset of G2/97 molecules as can be seen in Table **3-3**. Finally, we can conclude that our implementation is in good agreement with the literature results [9] and it can be used in a wide number of systems.

Table **3-1**: Grid-EDA total atomic energies versus Mulliken-type EDA calculation, the results are in a.u. In parenthesis we have the percentages of total HF molecular energy

	Oxygen		**Hydrogen**	
Basis set	**Mulliken-EDA**	**Grid-EDA**	**Mulliken-EDA**	**Grid-EDA**
Pople				
3-21G	-74.612391(98.71)	-74.411710(98.45)	-0.486509(1.29)	-0.586882(1.55)
6-31G	-75.048920(98.77)	-74.798025(98.44)	-0.467527(1.23)	-0.593024(1.56)
6-31G(d,p)	-75.0425557(98.71)	-74.851643(98.46)	-0.490286(1.29)	-0.585792(1.54)
6-311G	-75.0773958(98.77)	-74.821611(98.44)	-0.465983(1.23)	-0.593909(1.56)
6-311++G(d,p)	-75.0766750(98.72)	-74.867507(98.44)	-0.488077(1.28)	-0.592696(1.56)
Dunning				
cc-pVDZ	-74.961940(98.58)	-74.844084(98.42)	-0.540004(1.42)	-0.591557(1.56)
aug-cc-pVDZ	-74.961940(98.58)	-74.858902(98.44)	-0.540004(1.42)	-0.591567(1.56)
cc-pVTZ	-75.071506(98.70)	-74.881347(98.45)	-0.493088(1.30)	-0.588202(1.55)
aug-cc-pVTZ	-75.060573(98.68)	-74.880820(98.45)	-0.500268(1.32)	-0.590179(1.55)

Table **3-2**: Energy difference between the total HF energy in LOWDIN and the total energy of Grid-EDA

Basis set	**HF Energy (a.u.)**	**Grid-EDA Energy (a.u.)**	**Dif. (kcal/mol)**
Pople			
3-21G	-75.585409	-75.585474	0.040865
6-31G	-75.983974	-75.984073	0.061826
6-31G(d,p)	-76.023127	-76.023227	0.062441
6-311G	-76.009361	-76.009429	0.042794
6-311++G(d,p)	-76.052830	-76.052899	0.043048
Dunning			
cc-pVDZ	-76.027113	-76.027198	-0.053381
aug-cc-pVDZ	-76.041949	-76.042036	-0.054606
cc-pVTZ	-76.057681	-76.057751	-0.043906
aug-cc-pVTZ	-76.061109	-76.061178	-0.043426

Table **3-3**: Subset of G-2/97 molecules to compare total energies obtained with Grid-EDA and total HF energy of LOWDIN

Molecule	**HF Energy (a.u.)**	**Grid-EDA Energy (a.u.)**	**|Dif (kcal/mol)|**
H_2O	-76.023227	-76.023127	0.060453
LiH	-7.981366	-7.981187	0.109006
LiF	-106.934403	-106.934198	0.124646
Li_2	-14.866898	-14.866893	0.003240
HF	-100.011467	-100.011359	0.067904
NaCl	-621.399858	-621.399453	0.254222
CH_4	-40.201724	-40.201705	0.011667
CF_4	-435.644168	-435.644308	0.084889
$CHCl_3$	-499.096654	-499.095066	0.964648
H_2	-1.131278	-1.131278	0.000226
F_2	-198.674020	-198.673832	0.117820
CO	-112.737434	-112.737322	0.068043
CO_2	-187.632759	-187.632481	0.168893
C_2H_5OH	-154.086647	-154.086691	0.026730
HCOOH	-188.770819	-188.770566	0.158778
PH_3	-342.454358	-342.453527	0.504856
NH_3	-56.195180	-56.195200	0.012512
HCN	-92.875731	-92.875666	0.039489
CH_3CN	-131.762573	-131.762389	0.111785
CH_3NH_2	-95.221091	-95.221062	0.017936
SiH_4	-291.229917	-291.230819	0.547991
C_2H_2	-76.819706	-76.819700	0.003770
C_3H_6	-118.275776	-118.275817	0.025584
C_3H_8	-118.275797	-118.275842	0.027339
$CH_2CHCHCH_2$	-154.930204	-154.930324	0.075478

3.4.1 Grid points test

Standard grids for DFT calculations with the suitable numerical quadratures are well known [37, 45], however the accurate number of grid points when a new method or implementation arises is a matter of discussion. The recommended number of grid points reported by Nakai to have an equilibrium between chemical accuracy and numerical integration errors for small molecules is 94 points for the radial part (r) and 1152 (24,48) for the angular part where the numbers in parenthesis corresponds to θ and ϕ angles in spherical coordinates.

The results in Table **3-4** shows a relation between the number of grid points and the errors obtained by the difference between the total molecular energy of HF and the total molecular

energy obtained as the sum of the energy density analysis for water. From these data it is clear that the errors increase with the number of points. It is also worth to mention that a large number of points does not guarantee a better description of the phenomenon but it causes an increment in computing time, this happens because the singularities can not totally be neglected even if we use the PS method, furthermore the amount of integrals depends on the number of points.

Table **3-4**: Differences between total energy decomposition and total energy of LOWDIN using different number of grid points for H_2O at HF/6-311++G(d,p)

	Total Energies in a.u.			
Grid points	**Lowdin**	**Grid-EDA**	**Difference (kcal/mol)**	**J-K time (min)**
22650 (75/302)	-76.052830	-76.052899	0.043047	2.81
44250 (75/590)	-76.052830	-76.053020	0.118976	5.54
90150 (75/1202)	-76.052830	-76.053064	0.146587	11.81
115392 (96/1202)	-76.052830	-76.053303	0.296561	15.42
230550 (75/3074)	-76.052830	-76.053949	0.701932	27.57
277800 (75/3470)	-76.052830	-76.053966	0.712600	30.51

One question arises when we vary the number of grid points, that is, which is the energy decomposition term with the largest error. To solve this question we did a comparison between the Grid-EDA calculation with 22650 and 277800 grid points, both grids present the smallest and largest errors respectively. We take the grid with 22650 points as a reference point to perform the difference between each energy density component, from this difference the two-body interactions (J-K for Coulomb and exchange interactions) term have the largest error as it is shown in Table **3-5**, the number of integrals to solve in this part of the method causes the highest error accumulation.

Table **3-5**: Differences between total energy decomposition and total energy of LOWDIN using different number of grid points for H_2O at HF/6-311++G(d,p). The energy components are in a.u.

		Grid-EDA energy components			
	Atom	**Kin**	**JK**	**Ne (elec)**	**Ne (nuc)**
Grid points	O	74.842496	33.734425	-94.136848	-93.727633
22650	H	0.567899	2.017042	-2.678885	-2.883493
Grid points	O	74.842502	33.733355	-94.136849	-93.727634
277800	H	0.567899	2.017042	-2.678885	-2.883493
Differences	O	0.003765	-0.671435	-0.000628	-0.000628
(kcal/mol)	H	0.000000	0.000000	0.000000	0.000000

Based on these results we recommend the use of a Lebedev grid with 22650 points for its chemical accuracy and reasonable computing times.

3.4.2 Atomic radii tests

Different types of atomic radii are available to use in atomic size adjustment for heteronuclear molecules, these atomic radii are obtained experimentally and the origin of numerical differences among them relies on new experimental measurements and the inclusion of more molecules to average the radius per atom [39, 46].

The Bragg-Slater atomic radii is the most common set of parameters used to make an atomic size adjustment within Becke's space partitioning function. Although this set is widely used, other types of atomic radii can be considered. For example, a new set of atomic radii that results from an average of a large set of covalent and ionic molecules have been recently proposed by Cordero et. al.[46]. In our tests for atomic radii in Grid-EDA calculations we evaluated the differences in terms of atomic and total energies when we use Bragg-Slater or Cordero atomic radii modifying the atomic radii in Grid-EDA LOWDIN code (SEE APPENDIX of atomic radii).

For this comparison we selected water, hydrogen fluoride and sodium chloride because they are very different in their chemical nature (from covalent to ionic bonds) and their atoms have different values for Bragg-Slater and Cordero radii. These systems can give us an idea of how different is the energy decomposition, although they do not constitute a complete set of molecules to do a systematic evaluation of atomic radii suitability for Grid-EDA scheme.

In Table **3-6**, we show that similar percentages of total molecular energy are obtained using either Bragg-Slater or Cordero radii, however, the variations in total atomic energies between these radii are large. These large variations in atomic energies, are not a matter of concern since the partition is according to total molecular energy percentages.

Table **3-6**: Atomic energies comparison with Bragg-Slater and Cordero atomic radii

	Atomic radii in Å		**Atomic Energy in a.u.**	
Molecule	Bragg-Slater	Cordero	Atomic Energy (1)[1]	Atomic Energy (2) [2]
H_2O				
O	0.60	0.66	-74.851643 (98.46)	-74.910249(98.54)
H	0.35	0.31	-0.585792 (1.54)	-0.556515(1.46)
HF				
F	0.50	0.57	-99.399911(99.39)	-99.443964(99.43)
H	0.35	0.31	-0.611556(0.61)	-0.567502(0.57)
NaCl				
Cl	1.00	1.02	-459.445785 (26.06)	-459.465452 (26.06)
Na	1.80	1.66	-161.954073 (73.94)	-161.935423 (73.94)

[1] Atomic Energy (1): Total atomic energy of Grid-EDA using Bragg-Slater atomic radii
[2] Atomic Energy (2): Total atomic energy of Grid-EDA using Cordero atomic radii

Table **3-7**: Total energies comparison with Bragg-Slater and Cordero atomic radii

	Molecules		
Energies	**H_2O**	**HF**	**NaCl**
Total (1)[3] (a.u.)	-76.023227	-100.011467	-621.399858
Total (2)[4] (a.u.)	-76.023279	-100.011466	-621.400875
HF Energy (a.u.)	-76.023127	-100.011359	-621.399453
Diff.(1)[5] (kcal/mol)	0.062441	0.067904	0.254222
Diff.(2)[6] (kcal/mol)	0.095072	0.067276	0.892399

[1] Total (1): Sum of atomic energies using Bragg-Slater atomic radii
[2] Total (2): Sum of atomic energies using Cordero atomic radii
[3] Diff. (1): Difference between Total Lowdin energy and Total (1)
[4] Diff. (2): Difference between Total Lowdin energy and Total (2)

As we show in Table **3-7**, both Grid-EDA calculations are within chemical accuracy (< 1kcal/mol) when we compare the total molecular energy of Grid-EDA and the total molecular energy obtained in a HF calculation with LOWDIN. These results suggest that we could use either Bragg-Slater or Cordero atomic radii.
Three molecules for this comparison are not enough conclude about the best selection of atomic radii, in consequence, new systematic comparisons among atomic radii are needed. Finally, we recommend the use of Bragg-Slater atomic radii since it yields results within chemical accuracy and are they are widely used in the literature.

3.4.3 Code optimization

Computing time is an important factor in software implementation, to evaluate the most time consuming part of the method we added in Grid-EDA code the CPU time function of FORTRAN in each subroutine of the decomposition. From this, we identified that two-body interactions are the most time expensive energy terms to compute. The result is in accordance with Nakai's analysis since the computational cost of PS method for Coulomb and exchange energies is mn^2, where m is the number of grid points and n corresponds to the number of basis set functions [9].
As a first approximation for accelerating the code speed calculation, we decided to use a tool of FORTRAN compilers called screening. The results are presented in Table **3-8**, where the time is in seconds and the result for each basis set is an average of three calculations.

Table **3-8**: HF Grid-EDA Coulomb and exchange (J-K) time calculations for water molecule

	Time in seconds (s)		
Basis set	No Screening	Screening	Difference
6-31G	17.26	15.96	1.30
6-311G	38.75	35.19	3.56
6-311++G(d,p)	183.35	168.98	14.37

From these results we found that when we use the screening technique we can save around 8% of Coulomb and exchange time calculation. When we increase the basis set size, for example to *6-311++G(d,p)*, we saved around 14% of the time with respect to total no screening time calculation (Table **3-9**), with this result, we can infer that with larger basis sets the reduction in computing time is more valuable than with small basis sets.

Table **3-9**: Total time of Grid-EDA LOWDIN calculations

	Time in seconds (s)		
Basis set	**J-K Screening**	**Total time No Screening**	**% Saved time**
6-311++G(d,p)	168.98	196	13.79

Saving time is more important if we translate it in terms of larger systems than water. In our work we studied a problem related to biphenyl rotation but the number of atoms and the basis set used to obtain reliable results presented a limiting computing time case, i.e. 3.41 months for a system with just 22 atoms. To understand a bit more this problem, we present a graphic increasing the number of atoms in a series of unsaturated hydrocarbons and the computing time in minutes **3-7**.

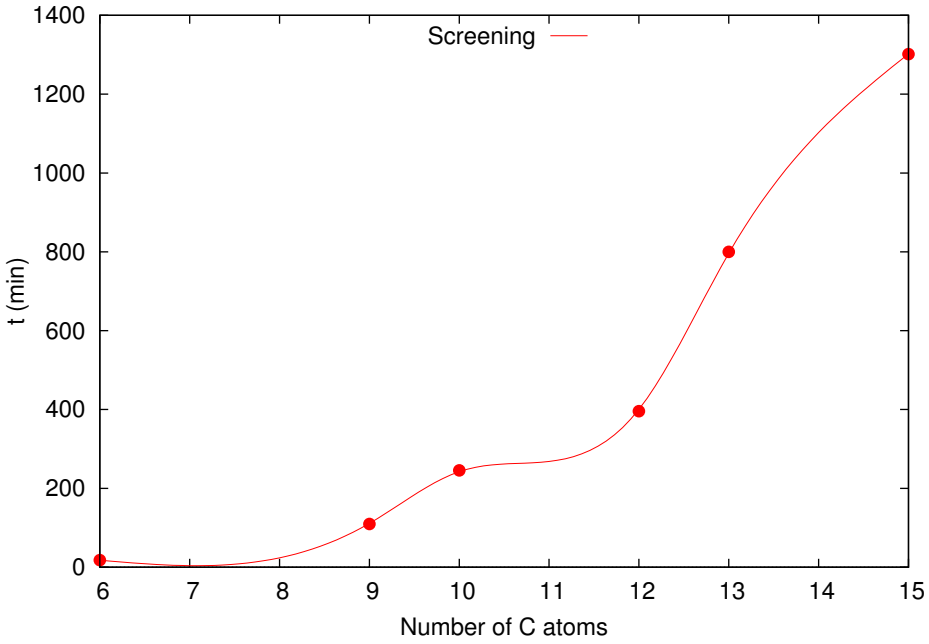

Figure **3-7**: Time computing tendency with an increasing number of atoms.

Table **3-10**: Time computing differences between No screening and screening.

Number of C atoms	**Difference (min)**
6	0.76
9	16.79
10	19.97
12	68.00
13	65.96
15	50.52

As we can see in the graphic, the computing time has a significant increase with respect to the number of atoms, we also notice that the reduction in time computing is greater for large than small systems as can be seen in Table **3-10**. Although we have reductions in computing

time using screening with an increasing number of atoms, this reduction is not significant for larger systems, for this reason we would need to implement paralellization techniques in future works.

4 Applications

In this chapter we present the application of Grid-EDA and Grid-EDA-APMO/HF to analyse the double proton transfer (DPT) process in formic acid dimer and to examine electronic changes in molecular systems in the presence of positrons.

4.1 Grid-EDA application

Double proton transfer in formic acid dimer

Double proton transfer processes are very important in chemistry and biochemistry since they are present in a wide variety of systems. For example, DPT undergoes in carboxylic acid dimers [47], nucleus base pairs (essential for DNA replication) and enzymatic reactions [48]. It also play important roles in the stability of transmembrane helix interactions [49] and transport through biological membranes[50].
Athough DPT has been extensively studied theoretically and experimentally it is not fully understood. Two points of discussion are considered to explain how DPT occurs i.e. its mechanism (concerted or stepwise)[51, 52] and the nature of the hydrogen bonds, that is, geometrical changes, physico-chemical properties and bond interactions (partially covalent or electrostatic)[53, 54].
Theoretically, DPT has been studied with time-independent and time-dependent *ab initio* methodologies [55]. *Ab initio* quantum dynamics can explain whether DPT is concerted or not in comparison with experimental studies and time-independent methods are used to discuss the geometry, physico-chemical properties and the covalent or electrostatic nature of the hydrogen bonds formed during DPT. To study the electrostatic or covalent interaction of chemical bonds we can use EDAM that focuses on the local rather than global energy changes in the molecule [56, 57].
Formic acid dimer is one of the most studied models where DPT occurs. It is well known that in this system the DPT is concerted, but the covalent or electrostatic interaction on its hydrogen bonds are matter of discussion. Therefore the relation between the atoms in the system during DPT remains unclear.
Hydrogen bonds are classified according to the bond strength and the interaction role they play within the molecules; thus, for the formic acid dimer they are classified as resonant-assisted hydrogen bonds (RAHBs), that is, a very strong hydrogen bond ($>$ 10 kcal/mol) [53]. The analysis of the electrostatic or partially covalent hydrogen bonds is motivated by

its relation with the different potential energy profiles in proton transfer processes. From the potential energy profiles in DPT, the geometry and the energy changes of the system are connected, that is for partially covalent or totally electrostatic interactions the potential curve may have changes from single to double wells along DPT[58].
In recent studies [56, 57], EDAM have been used to clarify the nature (partially covalent or electrostatic) of RAHBs. These studies focused on the partition of total molecular energy in intermolecular interaction energies. For example using block-localized wave function Beck et. al. proposed an EDAM that discussed the energy division in terms of electrostatic, Pauli repulsion, polarization and charge transfer effects [56].
From these terms they analyzed the cooperativity between $\pi - electron$ delocalization and the partial covalent nature of hydrogen bonds. They also quantified the resonance in the system finding that it has not a direct effect over hydrogen bonds. However, to study the nature of the formed hydrogen bonds, they noticed that the covalent interaction is mainly evaluated via intramolecular analysis (polarization and charge transfer).
To study in detail the covalency of hydrogen bonds one reasonable option is to decompose all atomic energy changes during a DPT. Recently, EDA methods have been proposed to decompose the atomic energy terms [8, 9], however, they have not been explored so far to analyse the possible connections between atomic energy changes and the nature of hydrogen bonds. One of the most important features of Grid-EDA consists on analysing the changes in atomic energy terms, that is, it offers the possibility to understand what changes undergo per atom during a DPT.
We want to use this methodology that has been validated in chapter 3 to decompose the total energy of formic acid dimer in gas phase. Our aim at decomposing its total energy is to describe the atomic energy density changes that affect the molecule during DPT, analyse its energy components and explore a new connection between these changes and the partially covalent or electrostatic nature of hydrogen bonds interactions. To perform a detailed description, the three stationary points of its intrinsic reaction coordinate (IRC) have been selected: the reactant, the product and the transition state (TS).

Methods

The IRC for DPT in formic acid dimer was calculated using the computational package GAMESS[42]. The structures for the stationary points were computed at HF/6-311++G(d,p) level of theory. The TS was characterized with only one imaginary frequency and its charecteristic normal vibration mode. After obtaining the geometries with GAMESS the analysis of Grid-EDA was performed at HF/6-311++G(d,p) level of theory in LOWDIN package.

Results and discussion

In Figure **4-1** we can observe the schematic representation of DPT in formic acid dimer. From this figure we see that the transferred atoms are those labeled with numbers 5 and 9

and the closest atoms involved in this transfer are oxygens labeled as 1, 4, 6 and 8.
In this process, we can identify oxygens 1 and 6 as donors and oxygens 4 and 8 as acceptors of hydrogen bonds when the DPT occurs. For data analysis we focus our attention on three aspects: the total atomic energy densities and geometrical changes, the population analysis, and finally the role of kinetic and potential atomic energies during DPT process.

Atomic energy densities and geometrical changes:
In formic acid dimer DPT, we have three significant geometry changes (Figure **4-1** and Table **4-1**): the first change is related to donor-proton and acceptor-proton bond distances, the second corresponds to the angles in reactant, transition state and product structures, and the last significant change corresponds to carbon and oxgygen bond distances (C-O and C=O distances are shown in Table **4-1**). These changes are considered in our analysis since the type of hydrogen bond changes with respect to modifications bond angles and distances [47].

Table **4-1**: C-O bond distances in reactant R, TS and P during formic acid dimer DPT.

	C-O distance in Å		
Bond	**R**	**TS**	**P**
C(2) -O(1)	1.299	1.239	1.190
C(2) -O(4)	1.190	1.239	1.299
C(7) -O(8)	1.190	1.239	1.299
C(7) -O(6)	1.299	1.239	1.190

To evaluate the effect of geometry changes over dimer atoms, we analyse differences in the atomic energy densities between TS and R and between P and R structures (see Table **4-3**). From these results we can observe that the largest energy changes are for donor, acceptor and the transferred atoms in TS-R change, for the other atoms the differences are negligible considering that the error in this system, that is the difference of Grid-EDA energy with respect to HF energy, is approximately 0.43 kcal/mol. For the global difference (P-R), the largest changes are for donor and acceptor atoms since the total change for protons are zero. These results allow us to determine that the donor atoms comprise the largest contribution to the barrier height ($\simeq$ 19.03 kcal/mol) followed by acceptors and the transferred protons. Therefore Grid-EDA allow us to determine the atoms that are directly involved in the DPT.

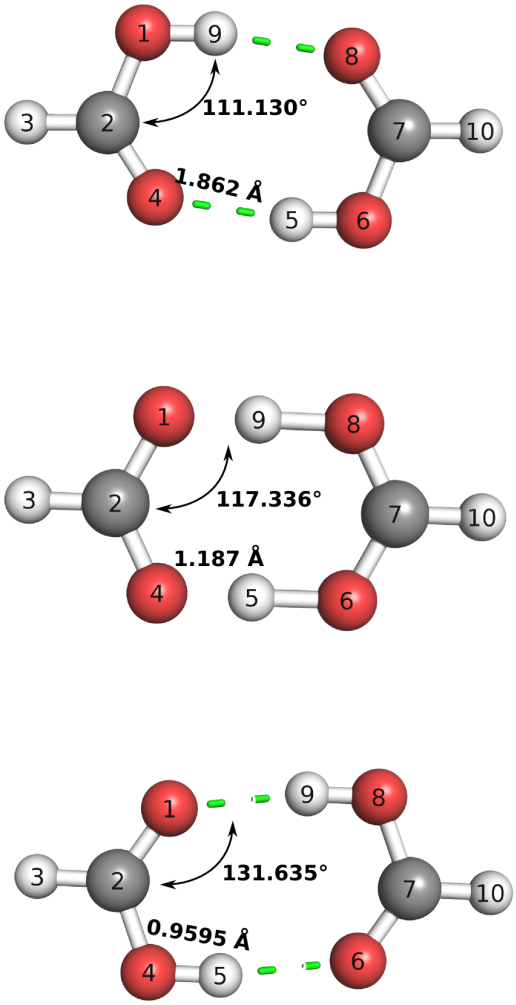

Figure **4-1**: DPT in formic acid dimer; the structures from top to bottom are reactant (R), TS and product (P). Colored balls represent the atoms: Oxygen (red), Carbon (grey) and Hydrogen (white)

Table **4-2**: C-O-H angles variation along DPT

	Angles for R, TS and P		
Angle	**∡ R**	**∡ TS**	**∡P**
C(2)-O(1)-H(9)	111.130°	117.336°	131.631°
C(2)-O(4)-H(5)	131.631°	117.336°	111.130°
C(7)-O(8)-H(9)	131.631°	117.336°	111.130°
C(7)-O(6)-H(5)	111.130°	117.336°	131.631°

Table **4-3**: Atomic energy densities and their differences for R, TS and P.

	Atomic energies in a.u.			**Differences in kcal/mol**	
Atom	**R**	**TS**	**P**	**TS-R**	**P-R**
O(1)(Donor)	-74.820671	-74.837995	-74.880561	**-10.871248**	**-37.581589**
C(2)	-38.005369	-38.006069	-38.005160	-0.439227	0.131073
H(3)	-0.548363	-0.547916	-0.548339	0.280327	0.014863
O(4) (Acceptor)	-74.880926	-74.837856	-74.820349	**27.027267**	**38.012821**
H(5) (Transfer)	-0.581388	-0.591747	-0.581331	**-6.500292**	0.035760
O(6) (Donor)	-74.820672	-74.837967	-74.880558	**-10.852787**	**-37.578955**
C(7)	-38.005368	-38.006071	-38.005156	-0.440914	0.132944
O(8) (Acceptor)	-74.880932	-74.837827	-74.820349	**27.048237**	**38.016236**
H(9) (Transfer)	-0.581385	-0.591747	-0.581336	**-6.502470**	0.030473
H(10)	-0.548362	-0.547912	-0.548339	0.282146	0.014288

We could determine that the donor atoms, O(1) and O(6), stabilize their atomic energy densities during the DPT while the opposite occurs for acceptors O(4) and O(8) (see Table **4-3**). This stabilization is associated to the formation of a double bond C = O after the proton transfer, the C=O formation is also seen in C-O bond distance shortening. The contrary undergoes for acceptor atoms (Figure **4-1**). The formation of C=O double bond is confirmed by the variation in the ∡ C-O-H where O is the donor atom and H is the atom involved in the transfer process. From Table **4-2** and Figure **4-1** we observe an increase in these angles from 111.1° to 131.6°. The first angle is close to the tetrahedral angle of 109.5°, it means that the oxygen keeps a sp^3 bonding with carbon and hydrogen atoms. The situation changes when the proton tranference has occured since the last angle is very close to 130°, this angle can be related to the C=O-H bond in formic acid monomer indicating that a sp^2 bond is formed.

These results suggest that the atomic energy stabilization/destabilization phenomena is mostly due to C-O interactions affected by the proton transfer. Considering the significant changes for oxygen atoms, a question may arise about the constant values of atomic energy densities for C atoms, but the explanation for this behavior relies on the unchanged chemical environment since they are attached to hydroxyl-carbonyl groups along the DPT.

Atomic populations:
The atomic population (N^A) analysis entails the reorganization of electron densities, in terms of bond breaking-formation process. In Table **4-4** we observe the atomic population changes along DPT in formic acid dimer. For TS-R differences we found that the largest variations in atomic populations occur in the donor atoms O(1) and O(6), it means that the eletronic density has increased around those atoms as a result of the formation of a double C=O bond and the proton transfer. The small decrease in the atomic populations of acceptor atoms and the transfer protons suggests the initial steps of a bond-formation process. Changes in the remaining atoms are negligible, this result is consistent with the unchanged atomic energy densities.
As DPT occurs between chemically equivalent donors and acceptor atoms of hydrogen bonds, the atomic populations have the same global change (P-R) with opposite sign i.e. an increase or a decrease in atomic populations. This result can be connected with the stabilizing/destabilizing atomic energy density changes, that is, the atoms that dicrease their energy densities are those forming C=O bonds. We noticed that the hydrogen bond formation in acceptor atoms also increases its atomic energy density and decreases its atomic population. The changes in atomic populations can be related with a first approach of sharing electrons in covalent bonds [59].

Table **4-4**: Atomic populations (N^A) and their differences between TS and R, and P and R.

	N^A			N^A differences	
Atom	**R**	**TS**	**P**	**TS-R**	**P-R**
O(1)	7.99	8.13	8.18	0.14	0.19
C(2)	6.05	6.06	6.05	0.01	0.00
H(3)	0.88	0.89	0.89	0.00	0.00
O(4)	8.18	8.13	7.99	-0.05	-0.19
H(5)	0.82	0.78	0.82	-0.04	0.00
O(6)	7.99	8.13	8.18	0.14	0.19
C(7)	6.05	6.06	6.05	0.01	0.00
O(8)	8.18	8.13	7.99	-0.05	-0.19
H(9)	0.82	0.78	0.82	-0.04	0.00
H(10)	0.88	0.89	0.89	0.00	0.00

The redistribution of electron density is also considered in other EDAM studies for instance Beck et. al. found that the increasing movement of π- electrons in the formic acid dimer to the carbonyl side affects molecular properties such as the magnitude of the dipole moment. Within their EDAM analysis, this increase in electron density is justified on conjugation effects present in RAHBs which affects the polarization and charge transfer energies related with a partial covalent nature of hydrogen bond [56].
Although the analysis of atomic population is a powerful tool to make relations between bond breaking-formation and stabilization/destabilization atomic energies, the changes in electron densities themselves do not give insights about the nature of hydrogen bond.

Kinetic and potential atomic energy densities:
Decades ago, the discussion about the electrostatic or partially covalent nature of hydrogen bonds was based on Hellman [60, 61] and Ruedenberg [62] statements. Hellman stated that the chemical bond is a cummulative electron density in the internuclear region whereas Ruedenberg concluded that "any explanation of chemical binding based essentially on an electrostatic, or other nonkinetic concept, misses the very reason why quantum mechanics can explain chemical binding whereas classical mechanics cannot".
Nowadays, new methodologies based on theoretical and experimental data discuss the interaction and classification of hydrogen bonds [53]. However the discussion of the electrostatic or partially covalent nature of hydrogen bonds has not finished [7, 63, 64, 65, 66, 67, 68].
In our work, we explore the features of Grid-EDA to discuss the electrostatic or partial covalent nature of double hydrogen bonds in formic acid dimer with respect to atomic kinetic and potential energy changes. We show in Table **4-5** the kinetic and potential atomic energy differences in two stages, TS-R and P-R. The energy differences in TS-R yields an increase in kinetic energy density for those atoms involved in bond breaking/formation (O(1), O(4), O(6) and O(8)), the increase in kinetic energy is also present in the transferred atoms H(5) and H(9), for those atoms where the kinetic energy increases the potential energy decreases. The global differences in atomic kinetic energies (P-R) clearly show that the atoms where a bond formation takes place also have an increase in their kinetic energies. Those atoms correspond to the oxygens that accept the hydrogen bonds. The atomic potential energies decreases for the donor atoms O(1) and O(6), this result explains their stabilization after bond breaking process.
In this bond breaking/formation process the method shows a relation with atomic kinetic and potential atomic energies, this is a unique feature of EDA method that may become an starting point to explore the relation between the atomic energy changes and the nature of hydrogen bond in this system·

Table **4-5**: Atomic energy differences in formic acid dimer during DPT

	Atomic energy density differences (kcal/mol)			
Atom	**Kinetic TS-R**	**Potential TS-R**	**Kinetic P-R**	**Potential P-R**
O(1)	33.000640	-43.871888	-21.345995	-16.235594
C(2)	-5.230013	4.790786	0.084005	0.047068
H(3)	0.402173	-0.121846	0.002030	0.012833
O(4)	54.355896	-27.328630	21.394852	16.617969
H(5)	-83.020181	76.519889	0.008167	0.027592
O(6)	32.997183	-43.849969	-21.354441	-16.224514
C(7)	-5.228333	4.787420	0.079356	0.053589
O(8)	54.363143	-27.314906	21.395131	16.621106
H(9)	-83.024146	76.521676	0.010736	0.019737
H(10)	0.398730	-0.116583	0.014870	-0.000583

From these results we propose to connect the nature of chemical hydrogen bond in formic acid dimer with Grid-EDA partition of energy for an A^{th} atom as follows:

$$\Delta^{Tot}E^{A} = \underbrace{(E_K(P) - E_K(R))}_{\text{Covalent part}} + \underbrace{(E_V(P) - E_V(R))}_{\text{Electrostatic part}}, \tag{4-1}$$

in this equation $E_K(P)$ and $E_K(R)$ are the atomic kinetic energies for the A^{th} atoms in products and reactants, and the terms $E_V(P)$ and $E_V(R)$ are the total atomic potential energy densities for the A^{th} atoms in products and reactants respectively.
The atomic total potential energy corresponds to:

$$^{Tot}E_V = E^A_{NN} + E^A_T + E^A_{Ne} + E^A_{clb} + E^A_{HFx}. \tag{4-2}$$

From the global (P-R) changes we determine the percentages of kinetic and potential energies associated with the covalent and electrostatic character of the hydrogen bonds in the molecular system (Equation 4-1). In Table **4-6** we found that for the atoms involved in the bond breaking-formation process, the covalent part is approximately 56% and the electrostatic part is approximately 44%.

Table **4-6**: Electrostatic and covalent character of hydrogen bonds in formic acid dimer DPT process

Atom	**% Covalent part**	**% Electrostatic part**
O(1)[Donor]	56.80	43.20
O(4)[Acceptor]	56.28	43.72
O(8)[Donor]	56.83	43.17
O(6)[Acceptor]	56.28	43.72

It is worth to mention that we are not relating these results with a final quantitative answer about the covalent or electrostatic nature of these bonds. However, we suggest that this method yields information about the covalent and electrostatic changes in the atoms directly involved in the proton transfer and from these results we infer that these type of hydrogen bonds are partially covalent in nature.
In future works, we will extend Grid-EDA to analyze not only atomic energies but binding molecular regions like Bond-EDA in the Mulliken approach [10].
In conclusion, the implementation of Nakai's method Grid-EDA is in agreement with the chemical picture of bond breaking-formation process, it is also a promising tool to study the nature of hydrogen bonds based on its atomic energy terms.

4.2 Grid-EDA-APMO/HF application

Positrons
In recent years, several studies have been carried out to explore the interactions and properties in positronic systems. For instance, the determination of positron binding energies [34, 33, 69] and molecular density changes [70, 71].
Experimental and theoretical studies clearly supports the attractive nature between positron and molecules. However, the information they produce do not explain completely the nature of attractive interactions. To understand the interactions between positron and molecules, we extend the idea of EDAM to exotic particles under APMO approach with the Grid-EDA-APMO/HF scheme. Our interest in extending Grid-EDA relies on the relations that can be formulated between chemical binding processes and atomic energy changes which is a unique feature of Grid-EDA method among others EDAM.
It is important to notice that this is the first attempt in decomposing the energy of a non conventional molecule in atomic energy terms; therefore, we expect to evaluate the strengths and weaknesses of our method in the challening task of solving questions about the positron-molecule interactions nature.
For Grid-EDA-APMO/HF tests, we have selected six diatomic heteronuclear molecules with one positron, all these systems are capable of binding positron based on the energy differences between the positronic system and the conventional molecule[34, 69].

Methods:
All Grid-EDA-APMO/HF calculations were performed with aug-cc-PVTZ electronic basis set in LOWDIN package. The molecular geometry and the location of the positronic basis set were selected according to previous studies, i.e. the positronic basis set was 7s7p7d and it was placed on the most electronegative atom [34].

Numerical assessment:
The reference value to validate the energy decomposition obtained with Grid-EDA-APMO/HF, is the APMO/HF energy resulting from LOWDIN package calculation. We consider that our systems are suitable for chemical analysis if the difference between Grid-EDA-APMO and APMO/HF energy is less than 1 kcal/mol .
In Table **4-7** we present the results for the positronic molecules. From these results we see that all seleted systems are within chemical accuracy. We also show that the energy of the positronic system is less than the energy of the conventional molecule as is expected for these positron binding systems.

Table **4-7**: Comparison between the total energies obtained with APMO/HF and the sum of atomic energies in Grid-EDA-APMO/HF. First column shows the differences between the total energies for the positronic and conventional systems. Fourth column corresponds to differences between APMO/HF and Grid-EDA-APMO. Differences are in kcal/mol.

	Energies in a.u.			
Molecule	**APMO/HF**	**HF -APMO/HF**	**Grid-EDA-APMO/HF**	**|Dif (kcal/mol)|**
BeO(e^+)	-91.297519	-1.886041	-91.297348	0.107440
CaO(e^+)	-756.367621	-4.800659	-756.367437	0.115762
LiO(e^+)	-82.271475	-0.389882	-82.270638	0.525193
MgO(e^+)	-277.867829	-3.490209	-277.866490	0.840322
NaO(e^+)	-237.048133	-0.682821	-237.049123	0.621255
LiH(e^+)	-8.485623	-0.499524	-8.485171	0.283507

Table **4-8**: Comparison between the total atomic energies between the molecule with positron and the molecule without positron. Differences are shown in kcal/mol.

		Atomic Energies in a.u.		
Molecule	**Atoms**	**Molecule(e^+)**	**Molecule(e-)**	**Diff kcal/mol**
BeO	O	-74.839205	-74.832993	-3.898086
	Be	-14.602714	-14.615994	8.333319
CaO	O	-74.82382	-74.816667	-4.488572
	Ca	-676.732741	-676.750295	11.015293
LiO	O	-74.250109	-74.249893	-0.135542
	Li	-7.631483	-7.631700	0.136169
MgO	O	-74.779327	-74.713608	-41.239264
	Mg	-199.584565	-199.664012	49.8537075
NaO	O	-74.323791	-74.323774	**-0.010668**
	Na	-162.041519	-162.041538	**0.011923**
LiH	H	-0.514500	-0.511069	-2.152983
	Li	-7.470002	-7.475030	3.155115

The negative differences for all systems are due to an stabilization energy with the positron. This decrease in the total energy can be related with a binding process between the molecule and the positron. Based on these variations a question arises about which changes are affecting each atom in the positronic system.

As can be seen in Table **4-8**, the atoms without the positronic basis set increase their atomic energy densities, whereas, for the atoms with the positronic basis set the opposite occurs. This increase/decrease of atomic energy densities undergo for all systems with the exception of NaO(e^+), where the atomic energy changes are negligible. Since this exception do not seem to have a simple explanation, we decided to go further in the analysis of the atomic energy densities and decompose them into kinetic, potential and coupling energy contributions, to have a better idea about the changes in the positronic system.

In Table **4-9** we observe an increase of atomic kinetic energy for those atoms where the positronic basis set was placed, however it decreases for the other atoms. This variation is small with respect to the atomic potential energies that decreases for all the atoms in the studied molecules. Although some authors connect the increase of kinetic energy with the formation of a chemical bond in conventional systems[68, 65], it is definitely the potential energy per atom in the positronic system that causes the energy stabilization with respect to the conventional molecule. From this result we have a first step in the explanation of positron binding to molecules.

An additional decrease in the positronic system energy with respect to the conventional molecule energy, can also be associated with the coupling term between positron and electrons since it presents an stabilizing effect over atomic energy densities (see Table **4-10**).We consider that our extension of the energy decomposition to systems with exotic particles, gives enough information to do a qualitative description about attractive interactions in the positron binding process, it also offers a connection between the atomic energy terms and the positron binding to molecules. In coming studies this connection can be the starting point to study sistematically positron binding to molecules. Finally, we recommend in future studies to perform the energy density analysis with a large set of molecules.

Table **4-9**: Atomic kinetic and potential energy densities differences between the molecule with positron and the molecule without positron. The differences are shown in kcal/mol.

		Atomic energy differences	
Molecule	**Atoms**	**Kinetic Dif (kcal/mol)**	**Potential Dif (kcal/mol)**
BeO	O	29.807305	-861.951379
	Be	-24.145291	-306.426556
CaO	O	66.161411	-1253.592665
	Ca	-10.037634	-1814.872364
LiO	O	0.646962	-173.248883
	Li	-0.350150	-71.176806
MgO	O	13.513406	-1159.348919
	Mg	-53.512085	-989.950522
NaO	O	0.419804	-174.068573
	Na	-0.405371	-255.043730
LiH	H	13.942622	-108.029267
	Li	-13.347744	-205.737057

Table **4-10**: Atomic kinetic and potential energy densities differences between the molecule with positron and the molecule without positron. The differences are shown in kcal/mol.

Molecule	**Atoms**	**Coupling atomic energy(e^+/e-) in a.u.**
BeO(e^+)	O	-1.315350
	Be	-0.540079
CaO(e^+)	O	-1.885140
	Ca	-2.925735
LiO(e^+)	O	-0.274843
	Li	-0.114204
MgO(e^+)	O	-1.760287
	Mg	-1.742311
NaO(e^+)	O	-0.276710
	Na	-0.407103
LiH(e^+)	H	-0.146507
	Li	-0.354162

5 Conclusions and perspectives

In this work we presented the implementation of Grid-EDA and its theoretical extension within the APMO approach in LOWDIN. For this purpose, we have developed the mathematical expressions for decomposing the coupling term over the total APMO/HF energy in non-conventional molecules.

We have performed two applications in our implementation. The first application regarded to a double proton transfer process in formic acid dimer. Along this process, the changes in kinetic and potential atomic energies suggested a connection between the covalent and the electrostatic nature in RAHBs.

The second application considered the energy density analysis in six positronic systems with Grid-EDA-APMO/HF. Two important lessons came from this extension. The first lesson was that Grid-EDA-APMO/HF is cappable of produce information about attractive interactions between the positrons and the atoms. Furthermore, the atomic energy terms could be analysed in a chemical binding process, thus; the kinetic and potential energy terms are proposed as indicators of attractive interactions, since the atomic kinetic energy increases its value in the atom with the positronic basis set, the potential and coupling atomic energy decrease allows to explain the stabilizing total energies for the positronic system against the conventional diatomic molecule. We also observe that the atomic potential energy terms are the largest contributions in the stabilizing process of positron-molecule interactions.

The second lesson have to do with the possible limitations or unexplained results of the extension. For example, in the positronic systems there are not trend within the atomic coupling energies. Additionally, for $NaO(e^+)$, the total atomic energy differences with the conventional molecule are not significant, although, the kinetic and potential energy changes are consistent with all the study systems. These effects arise questions about the type of chemical differences between these non-conventional systems. To solve the possible questions about this phenomenum we recommend to compute Grid-EDA with more positronic systems and consider other properties in the analysis e.g. positron binding and positron affinity energies.

Based on our analysis, we focus in the perspectives and possible extensions of this work with other methodologies. In future works we are interested in the inclusion of electron correlation for both Grid-EDA and and Grid-EDA-APMO. The addition of electron correlation in Grid-EDA within DFT methodology needs the inclusion of functionals in LOWDIN. For post-Hartree-Fock methods this topic requires more discussion. We are also interested in the extension of Grid-EDA to study solvated systems with the Conductor-like screening model

(COSMO), since this method was recently extended to treat multiple type of quantum species in our research group. Finally, to analyse larger systems, we can connect Grid-EDA with Quantum mechanics/Molecular mechanics QM/MM.
In conclusion, Grid-EDA and Grid-EDA-APMO/HF are promising tools to study the chemical nature of binding processes in a wide variety of systems from conventional and non-conventional systems.

Bibliography

[1] K. Gavroglu and Sim Oes. *Neither physics nor chemistry: a history of quantum chemistry.* (The MIT press, 2012).

[2] P.K. Chatarraj. *Chemical reactivity theory: A density functional view.* (CRC press, 1997).

[3] J.F. Gonthier, S.N. Steinman, M.D. Wodrich, and C. Corminboeuf. *Chem. Soc. Rev.*, **41**, 4671, 2012.

[4] P. Su and H. Li. *J. Chem. Phys.*, **31**, 014102, 2009.

[5] K. Morokuma and K. Kitaura. *lnt. J. Quantum Chem.*, **X**, 325, 1976.

[6] I. Mayer and A. Hamza. *Theor. Chem. Acc.*, **105**, 360, 2001.

[7] P. Salvador and I. Mayer. *J. Chem. Phys.*, **120**, 5046, 2004.

[8] H. Nakai. *Chem. Phys. Lett.*, **363**, 73, 2002.

[9] Y. Imamura, A. Takashi, and H. Nakai. *J. Chem. Phys.*, **126**, 034103, 2007.

[10] H. Nakai and Y. Kikuchi. *J. Chem. Theory*, **4**, 317, 2005.

[11] Y. Yamauchi, S. Ozawa, and H. Nakai. *J. Phys. Chem. A*, **111**, 2062, 2007.

[12] H. Sato and S. Ozawa, Sakaki. *J. Phys. Chem. A*, **108**, 1629, 2004.

[13] H. Sato, F. Hirata, and S. Sakaki. *J. Phys. Chem. A*, **108**, 2097, 2004.

[14] Y. Imamura, T. Baba, and H. Nakai. *lnt. J. Quantum Chem.*, **108**, 1316, 2008.

[15] Y. Kawamura and H. Nakai. *J. Comput. Chem.*, **25**, 1882, 2004.

[16] T. Baba, M. Ishii, Y. Kikuchi, and H. Nakai. *Chem. Lett.*, **36**, 616, 2007.

[17] Y. Kawamura and H. Nakai. *Chem. Phys. Lett.*, **410**, 64, 2005.

[18] H. Nakai and Y. Kikuchi. *J. Comput. Chem.*, **27**, 8, 2006.

[19] Y. Yamauchi and H. Nakai. *J. Electrochem. Soc.*, **160**, A1364, 2013.

[20] H. Nakai and K. Sodeyama. *THEOCHEM*, **637**, 27, 2003.

[21] Takeuchi M., A. Nakata, and H. Nakai. *Chem. Lett.*, **34**, 844, 2005.

[22] F. Moncada, L. Uribe, J. Romero, and A. Reyes. *lnt. J. Quantum Chem.*, **113**, 1356, 2013.

[23] M. Tachikawa. *Chem. Phys. Lett.*, **360**, 494, 2002.

[24] H. Nakai. *lnt. J. Quantum Chem.*, **107**, 2849, 2007.

[25] P.S. Webb, T. Iordanov, and S. Hammes-Schiffer. *lnt. J. Quantum Chem.*, **117**, 4106, 2002.

[26] Jean Y.C., P.E. Mallon, and D.M. Schrader. *Principles and applications of positron and positronium chemistry*. (World Scientific, 2003).

[27] W.C. Walker. *Muon and Muonium Chemistry*. (Cambridge University Press, 2009).

[28] González S.A., Aguirre N.F., and A. Reyes. *lnt. J. Quantum Chem.*, **108**, 1472, 2008.

[29] J. Romero, Reyes A., and J. Wist. *Spectrochim. Acta Mol.*, **77**, 845, 2010.

[30] D. Moreno, González S.A., and Reyes A. *J. Chem. Phys*, **134**, 024115, 2011.

[31] F. Moncada, D. Cruz, and A. Reyes. *Chem. Phys. Lett.*, **539**, 209, 2012.

[32] E. Posada, F. Moncada, and A. Reyes. *J. Phys. Chem. A*, **118**, 9491, 2014.

[33] J. Charry, J. Romero, M.T.do.N. Varella, and A. Reyes. *Phys. Rev. A At. Mol. Opt. Phys.*, **89**, 052709, 2014.

[34] J. Romero, J. Charry, R. Flores-Moreno, M.T.do.N. Varella, and A. Reyes. *J. Chem. Phys.*, **141**, 114103, 2014.

[35] R. Flores-Moreno, E.F. Posada, F. Moncada, J. Romero, J. Charry, M.A. Díaz-Tinoco, González S.A., Aguirre N.F., and A. Reyes. *lnt. J. Quantum Chem.*, **114**, 50, 2014.

[36] A.D. Becke. *J. Chem. Phys.*, **8**, 2547, 1986.

[37] C.W. Murray, N.C. Handy, and G.J. Laming. *J. Chem. Phys.*, **78**, 997, 1993.

[38] Mulliken R.S. *J. Chem. Phys.*, **28**, 1833, 1955.

[39] J.C. Slater. *J. Chem. Phys.*, **41**, 3199, 1964.

[40] R.A. Friesner. *Chem. Phys. Lett.*, **116**, 39, 1985.

[41] R. Flores-Moreno, J.M. Del Campo, and T. Ida. Available at https://sites.google.com/site/gdlquantumchemistrygroup/home/software/parakata. Last accessed 2013/06/21., 2008.

[42] M. Schmidt, K. Baldridge, K. Boatz, S. Elbert, M. Gordon, J. Jensen, S. Koseki, N. Matsunaga, K.A. Nguyen, S. Su, T. Windus, M. Dupuis, and J. Montgomery. *J. Comput. Chem.*, **14**, 1347, 1993.

[43] L.A. Curtiss, K. Raghavachari, P.C. Redfern, and J.A. Pople. *J. Chem. Phys.*, **106**, 1063, 1997.

[44] A.R. Hoy and P.R. Bunker. *J. Mol. Spectros.*, **74**, 1, 1979.

[45] M.W. Gill, G.J. Johnson, and J.A. Pople. *Chem. Phys. Lett.*, **209**, 506, 1993.

[46] B. Cordero, V. Gómez, A.E. Platero-Prats, M. Revés, J. Echeverría, E. Cremades, F. Barragán, and S. Alvarez. *Dalton Trans.*, **2833**, 2832, 2008.

[47] S.J. Grabowski. *Hydrogen bonding - New insights, in challenges and advances in computational chemistry and physics.* (Springer, 2006).

[48] M. Shibata, T.J. Zielinski, and R. Rein. *In theoretical biochemistry and molecular biophysics.* (Guilderland, 1991).

[49] A. Senes, I. Ubarretxena-Belandía, and D. Engelman. *Proc. Natl. Acad. Sci. U.S.A.*, **98**, 9056, 2001.

[50] V. Hrouda, J. Florian, M. Polasek, and P. Hobza. *J. Chem. Phys*, **98**, 9922, 1994.

[51] Z. Smechardina, W. Siebrand, and A. Fernández-Ramos. *J. Chem. Phys.*, **127**, 174513-1, 2007.

[52] S. Schweiger and G. Rauhut. *J. Phys. Chem. A*, **110**, 2816, 2006.

[53] G. Gilli and P. Gilli. *J. Mol. Struct.*, **552**, 1, 2000.

[54] S.J. Grabowski and J.M. Ugalde. *Chem. Phys. Lett.*, **493**, 37, 2010.

[55] T. Loerting and K. Liedl. *J. Am. Chem. Soc.*, **120**, 12595, 1998.

[56] J.F. Beck and Y. Mo. *J. Comput. Chem.*, **28**, 455, 2007.

[57] A. Smaga and J. Sadlej. *Comp. Theor. Chem.*, **998**, 120, 2012.

[58] G. Gilli and P. Gilli. *The nature of the hydrogen bond: Outline of a comprehensive hydrogen bond theory.* (Oxford Science Publications, 2009).

[59] G.N. Lewis. *J. Am. Chem. Soc.*, **38**, 762, 1916.

[60] H. Hellman. *Z. Phys.*, **85**, 180, 1933.

[61] C.A. Coulson. *Valence*. (Oxford University Press, 1961).

[62] K. Ruedenberg. *Rev. Mod. Phys.*, **34**, 326, 1962.

[63] W. Kutzelnig. *Angew. Chem., Int. Ed. Engl.*, **12**, 546, 1973.

[64] C. Esterhuysen and G. Frenking. *Theor. Chem. Acc.*, **111**, 381, 2004.

[65] I. Mayer. *Simple theorems, proofs, and derivations in quantum chemistry*. (Springer, 2003).

[66] G.B. Bacskay and S. Nordholm. *J. Chem. Phys*, **117**, 7946, 2013.

[67] I. Mayer. *J. Phys. Chem. A*, **118**, 2543, 2014.

[68] K. Ruedenberg and M.W. Schmidt. *J. Phys. Chem. A*, **113**, 1954, 2009.

[69] R.J. Buenker, H.P. Lieberman, and V. Melnikov. *J. Phys. Chem. A*, **109**, 5956, 2005.

[70] T. Oyamada and M. Tachikawa. **109**, 5956, 2005.

[71] G.F. Gribakin, J.A. Young, and C.M. Surko. *Rev. Mod. Phys.*, **82**, 2557, 2010.